1 Introduction

Modern digital acquisition systems (broadband sensors, timing with GPS or DCF-systems, sampling rates $\geq$ 80 Hz) and the use of modern analyzing software allow arrival-time determination of seismic signals with a precision of up to a few tenth of milliseconds. To benefit from this advancement in travel-time based methods like earthquake location and seismic tomography, consistent arrival time determination and error assessment (including uncertainty estimates of timing and phase interpretation) is crucial. Uncertainties of the arrival-time determination have to be provided in order to weight the data properly in the inversion procedure, i.e. arrival-time picks of high quality contribute more to the solution than those of low quality. The impact of such consistently picked and weighted data on tomographic models has recently been shown by several studies (e.g. Di Stefano et al. 2006, Diehl et al. 2009, Husen et al. 2009).

Although seismic arrival times represent the fundamental data of many seismological applications, the description of consistent phase picking receives only little attention. Simon (1981) and Kulhánek (1990 and 2002) provide a general overview about seismogram

interpretation from local to teleseismic scales. They focus mainly on basic descriptions of phases observable in common seismograms. The assessment of timing uncertainty and phase interpretation, however, is barely discussed. The fundamentals of digital signal processing and their influence on onset properties are described, e.g., in Seidl and Stammler (1984), Scherbaum (2001), and Scherbaum (2002). Among the few recent guidelines, the first edition of the *New Manual of Seismological Observatory Practice* (NMSOP) provides in Chapter 11 (Bormann et al., 2002) already an introduction to basic picking principles for local, regional and teleseismic seismograms, proposing the quantification of the onset-time reliability, yet a detailed description for consistent quality assessment is missing, similar to the discussion in Scherbaum (2001).

This tutorial is intended to provide a more detailed description on seismic phase picking. Basic principles (including a consistent quality assessment for timing uncertainty and phase interpretation) and common pitfalls of manual picking are described in section 2. In section 3, we present a practical procedure for consistent hand picking. The proposed method is especially intended for picking a reference data set for testing and calibrating of automatic picking algorithms, as described in Chapter 16 of NMSOP-2. The tutorial is focused on crustal and upper mantle phases of local and regional seismic events, recorded at epicentral distances from a few 10 km to several 100 km. But the outlined principles apply likewise to teleseismic records, however, then for different time and frequency resolution and recording bandwidth.

2   Routine hand picking

Especially for local and regional earthquake data, phase picking often becomes inconsistent and ambiguous due to rather complex waveform patterns and the close arrival of different phase types within a short time period of the same coda. In general, the shape of a seismic wavelet is affected by the source time function, the radiation pattern, dispersion, attenuation, scattering, interference with other phases, the signal-to-noise ratio (SNR) at the recording site, and the response characteristic of the recording system. The superposition of these components may lead to highly complex waveforms in case of high-frequency local and regional recordings. Moreover, the picking of later phases such as PmP or S-waves becomes even more difficult, since they interfere with the coda of earlier phases. Since the target accuracy of such arrivals is usually within few hundred milliseconds, errors like phase misinterpretations denote blunders and may significantly bias hypocenter locations and velocity models derived from onset-time observations. Furthermore, regional studies usually require the compilation of data from several networks. In such a case, merging routinely measured phase data will add even more inconsistency.

The possible sources for inconsistent hand picking described in the following sections refer mainly to P-wave picking. However, the basic principles of picking and error assessment of phases are also valid for S-wave picking. In addition, section 2.6 includes problems specific to S-wave picking.

In general, a seismic phase is defined by two visual observations:
1. Change primarily in amplitude:
     The amplitude exceeds the background noise (for a certain amount of time). This can also be denoted as amplitude based signal-to-noise ratio (*ASNR*). We may define a phase, if its amplitude exceeds the background noise at least by a factor of 1.5 (*ASNR*

$\geq$ 1.5). Figure 1 represents a typical example for a phase arrival defined by a change of the *ASNR*.

2. Change primarily in frequency:
    A change of the dominant frequency indicates the arrival of a seismic phase. We can refer to this observation as frequency based signal-to-nose ratio (*FSNR*). Unlike the *ASNR*, it is often much more difficult to quantify visually. Moreover, the dominant frequency of noise and signal can sometimes be very similar. But especially for broad time windows, the *FSNR* can help to determine the approximate position of a phase. Figure 2 represents a typical example for a phase arrival defined by a change of the *FSNR*.

Once a phase is recognised based on *ASNR* or on *FSNR* or - most likely - a combination of both, we have to determine the precise wavelet onset ('arrival time'). However, its position is usually not completely independent from the associated overall observation uncertainty. Finally, we have to identify the phase type and to do so, we have to answer questions like: May we assign the ray path to the phase (Pg, Pn, PmP) with certainty or is the station near a triplication point (see Chapter 2, Figs. 2.29 and 2.40)? Are we sure that it is the first arrival or is it possible, that an earlier phase is hidden in the noise? In addition, the visual examination of *ASNR* and *FSNR* can be rather subjective and strongly depends on the width of the used time window and also on amplitude scaling. Finally, filtering can affect *ASNR* and *FSNR* significantly. In the following sections, we will give examples for these problems and suggest possible solutions in order to minimize inconsistencies during the picking process. Once identified, it should be possible to minimize their contribution by defining certain rules and procedures, which finally add up to a consistent picking workflow and consistent uncertainty assessment for each observation.

2.1 Phase Picking Part I: Phase timing and its error assessment

The basic quantities associated with a picked phase are usually the absolute arrival time and the corresponding observation error. However, it is difficult or even impossible to give a general definition of a seismic onset, which could be used for the actual measurement of first arrival time from a sampled band-limited signal in the presence of noise (Seidl and Stammler 1984). Therefore, the visual determination of absolute arrival times often implies a high degree of subjectivity and inconsistency. Consequently, a physical consistent formulation can only be achieved by a probabilistic point of view. Such an approach directly relates the measured arrival time with the corresponding observation error. Considering the onset of a seismic phase as probabilistic function $P_a(t)$, the arrival time is expressed as the "most likely" time t_A, with $P_a(t_A)=Max(P_a)$. On the other hand, the 'earliest' possible time for the phase onset is defined as t_E, where the likelihood for onset is approaching zero. Thus $P_a(t_E) \geq 0$. Similarly, the 'latest' possible time for the phase onset t_L, is defined as $P_a(t_L) \geq 0$.

Figure 1 illustrates the proposed concept for a typical *ASNR*-case in further detail. Although the onset of the phase is rather impulsive and exhibits an almost ideal SNR, it is difficult to determine an arrival time consistent with picks of waveforms from the same seismic source recorded at other stations. The thick grey band between position '1' and '2' defines the time window that for certain includes the onset of the wavelet. The band outlined by two broken lines denotes the possible threshold of the noise amplitude. In practice, we first determine the position of t_L and t_E. For a consistent determination of t_L and t_E, we have to setup a common

procedure. Since the amplitude exceeds the threshold several times at position '2', the end of the grey band is certainly too late to be picked as t_L. Therefore, we define the intercept between signal amplitude and the a priori noise threshold (here: 1.5 times the largest noise amplitude in the noise-measurement time window) as t_L. Usually, the consistent determination of t_E is more difficult. In Figure 2 we fit a tangent (dashed line 'a') to the smoothed slope of the onset. If we shift the tangent from t_L towards earlier times, the slope decreases. The earliest possible time t_E corresponds with the first zero slope from t_L towards earlier time. Therefore, the start of the grey band (position '1') is certainly too early and on the other hand, t_A would be too late to be picked as t_E. To ensure t_E includes the zero slope time in the presence of larger background noise, we could shift it to earlier arrival by approximately half a wavelength of the dominant noise. Subsequently, we pick the arrival of the phase at the most likely position t_A, within the error interval of t_E and t_L (e.g on the seismogram's leading edge). For the special case of an ideal delta-pulse, t_E and t_L would coincide with t_A.
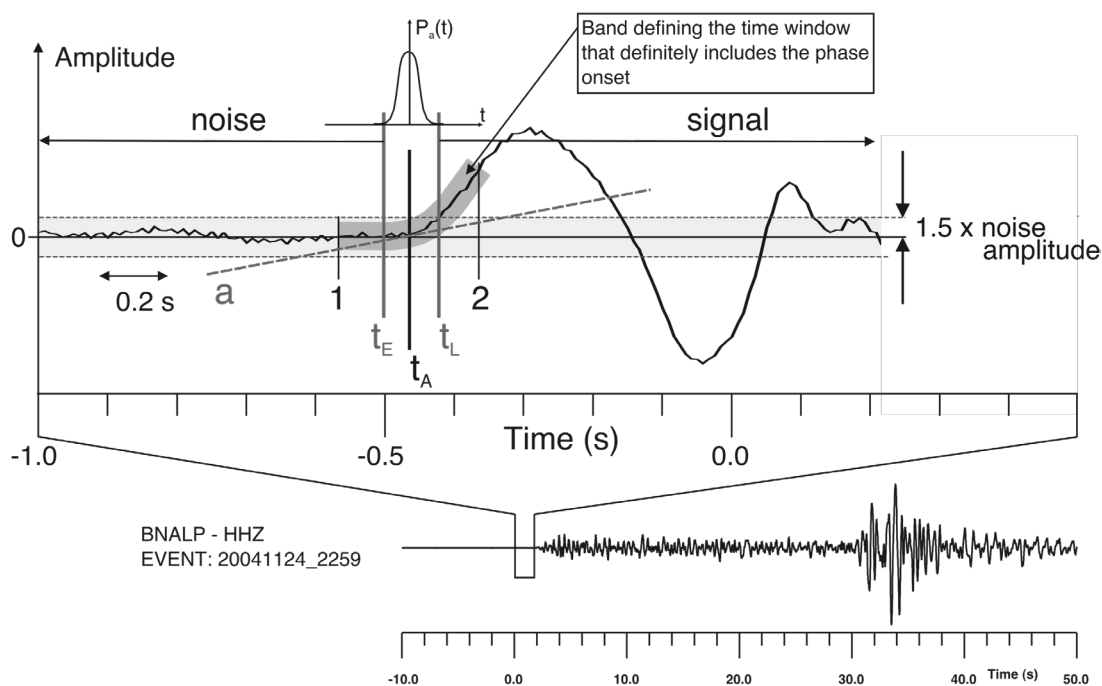

Figure 1   Probabilistic phase picking approach based on change of *ASNR*: the 'earliest' possible pick corresponds to t_E, the 'latest' possible pick corresponds to t_L. The most likely arrival time t_A is located within this interval. Primarily amplitude is used for determination of t_E and t_L. Copy of Fig. 2 in Diehl et al. (2009, p. 544) with © granted by the Geophysical Journal International.

Figure 2 illustrates a possible concept for the *FSNR*-case. Again, the thick grey band between position '1' and '2' defines the time window that for certain includes the onset of the wavelet and the band outlined by two broken lines denotes the possible threshold of the noise amplitude. The change in frequency is obvious for arrival times greater then position 'b'. Therefore, we define t_L a quarter signal wavelength ($\lambda/4$) after position 'b'. For arrival times earlier than position 'a', the signal frequency, which dominates the grey-banded wavelet after position b, is certainly no longer recognizable. Therefore, we pick t_E half a signal wavelength ($\lambda/2$) before position 'a'.

The consistent determination of t_A in the ASNR as well as in the FSNR case can be difficult and might include some degree of subjectivity in practice. Although t_A in Figure 1 and 2 seems to be located halfway between t_E and t_L, a symmetrical distribution is not always appropriate and in some cases, a highly asymmetrical distribution is required (especially for broadband records). There is no universal definition for determination of t_A, but its position usually coincides with a prominent kink or discontinuity in the waveform, separating the noise from the signal. The position of t_E should include all possible earlier onsets of the picked phase. In that sense the utmost precision of t_A is less crucial as long as it is included in an appropriate uncertainty interval.
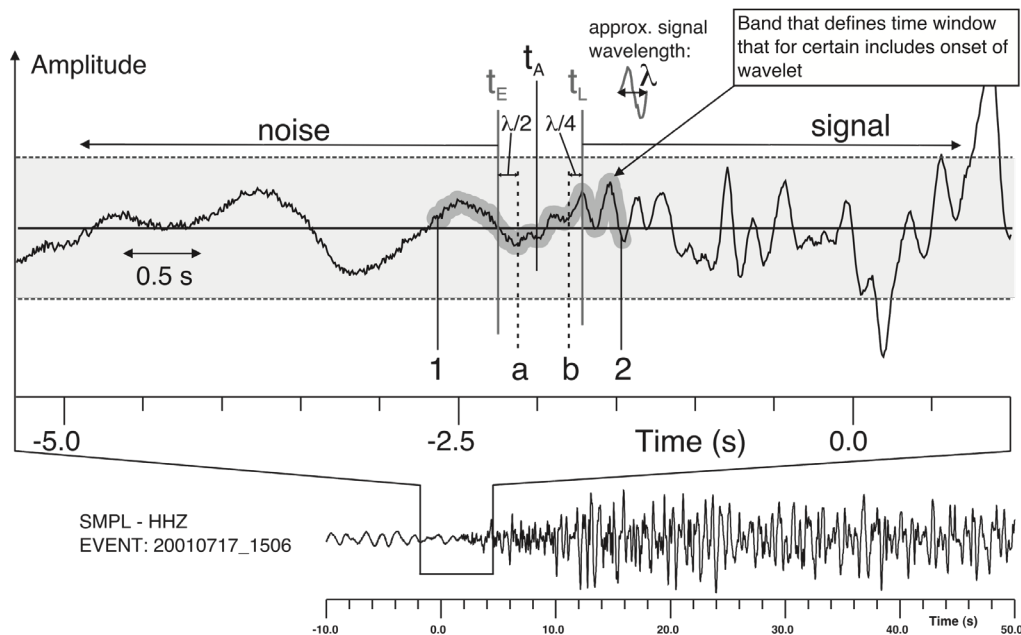

Figure 2   Probabilistic phase picking approach based on change of *FSNR*: the 'earliest' possible pick corresponds to t_E, the 'latest' possible pick corresponds to t_L. The most likely arrival time t_A is located within this interval. Primarily frequency is used for determination of t_E and t_L.

Usually, the observation error is related with a discrete weighting or quality class (e.g. 0-5). However, these classes are often traditionally defined only through qualitative attributes, like waveform shape (impulsive or emergent). Such classification is not longer sufficient for a consistent error assessment. Instead, a quantitative weighting scheme has to be defined, which assigns the weighting class depending only on the measured time error interval t_L-t_E. In addition, the measurement of t_L, t_E, and t_A allows us to adjust the weighting class definition even after the picking process. Finally, the availability of uncertainty intervals offers the possibility to assess the performance of automatic picking algorithms in a quantitative sense. Phase picks of automatic algorithms are expected to fall within uncertainty intervals of the corresponding manual picks. For more details on test and calibration of automatic algorithms see Chapter 16.

5

2.2 Phase Picking Part II: Phase identification and its error assessment

Although phase misinterpretation can result in significantly large errors, phase identification is typically not supplied with any observation error or uncertainty attribute at all (unlike arrival time of a phase). As demonstrated by synthetic travel time curves in Figure 3, the first arrival of the local or regional P-wave prior to its related coda is usually either Pg (direct wave as illustrated in the inset of Fig. 3) or Pn (Moho-refracted wave). Whether Pg or Pn is the first arriving wave depends on epicentral distance Δ, crustal thickness z_M, and focal depth z_F. As a rule of thumb, Pn from a surface focus takes over Pg at $\Delta \approx 5\, z_M$, for deeper sources, however, at shorter distances. Also Moho tilt and the direction of observation with respect to the direction of Moho dip influence both the slope of the Pn travel-time curve and the "take-over" distance (for both effects see Chapter 2, Fig. 2.40).
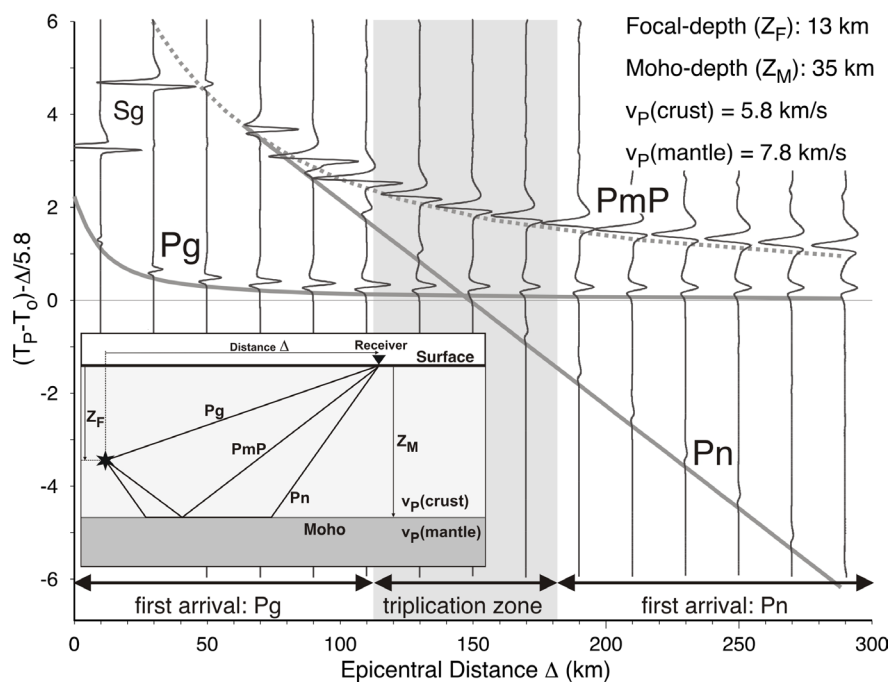

Figure 3 Reflectivity seismograms (vertical components) and synthetic travel time curves (solid and dashed lines) for main phases observed in local and regional earthquakes (one layer over half space). Focal depth is set to 13 km and time axis is reduced by 5.8 km/s. Phase identification is expected to be difficult in the distance range of phase triplication. The position and width of this zone mainly depends on focal depth and Moho topography.

Moreover, the discrimination between Pg and Pn can become rather difficult in the distance range of phase triplication (see Fig. 3 as well as Figs. 2.28b, 2.29 and 2.40 with related texts in Chapter 2). The Moho-reflected PmP phase always arrives after Pg and Pn, although its amplitude can become the dominant phase in the coda. The synthetic reflectivity seismograms (Fuchs and Müller, 1971) in Figure 3 illustrate the theoretically expected amplitude ratios between Pg, Pn, and PmP for a simplified crustal model using a moment tensor as a source.

According to it, especially for large epicentral distances, Pn can be expected to be masked in the presence of noise and Pg or PmP then likely to be misinterpreted as the first arrival.

6

However, Figure 4 presents a velocity-reduced real record section and the related travel-time curves for Pg, Pn and Pm from a local earthquake near Walenstadt, Switzerland with a focal depth of 13 km. It looks very different from the synthetics in Figure 3, calculated for a source at the same depth in the same simplified crustal model. From this it is obvious that, based on synthetic waveform characteristics alone, phase interpretation is rather difficult. Real records of seismic waves that have been radiated by extended seismic sources and travelled through complex media, resulting in multi-pathing and long codas, may look very different. In Figure 4 this holds especially for records at some stations in the distance range of phase triplication (e.g., station SPAK and SIERE). Also the amplitude ratio between Pg and Pn exhibits strong variations between some stations (e.g., EMV and HEI), probably due to 3D Moho topography and/or the influence of the source radiation pattern, which effects the Pn/Pg amplitude ratio because of the rather different take-off angles of these two waves from the source. Whereas in the case of EMV Pn is likely to be missed and Pg be picked as first arrival phase Pn is an unexpectedly large and sharp onset at station HEI. Moreover, for distances above some 400 km there is a tendency of Pn (which then becomes more and more a diving phase in the uppermost mantle, usually not modelled by any synthetics) to have larger amplitudes than Pg, which is more strongly attenuated and/or scattered in the more complex upper crust. This is illustrated by many record examples in DS 11.1. Similarly, as obvious from Figure 4, the determination of the phase type from generalized waveform features alone can also be rather ambiguous in the range of the crossover distance between Pg and Pn.

Since most applications like hypocenter localisation and travel-time tomography are (still) based on first arrivals only, an assessment for phase identification should avail of some guidance to avoid inconsistencies. The relevance of correct phase interpretation becomes even more evident for S-wave picking (see section 2.6). For use in routine first-arrival studies and subsequent special tomographic studies at local to regional distances, we therefore propose to identify crustal phases according to the rough waveform characteristics outlined below and to decide about their suitability for first arrival studies according to the assessment scheme presented in Table 1.

Table 1 Suitability assessment scheme of crustal phases for routine first arrival studies.

Phase label	Phase is…	Phase used for routine 1st arrival studies
Pg, Sg	Direct (crustal)	Yes (if first arrival)
Pn, Sn	Moho-refracted	Yes (if first arrival)
PmP, SmS	Moho-reflected	No
P1, S1	Unknown type, but certainly first arrival	Yes
P2, S2	Unknown type, second arrival	No
P3, S3	Unknown type, third arrival	No
P, S	Unknown type, uncertain if first arrival	No

- **Pg**: Impulsive high-frequency onset. At short distances, absorption is small and dispersion tends to sharpen the wavelet front (Seidl and Stammler 1984). Pg is first arrival close to epicenter.

- **Pn**: Usually with small amplitude at $\Delta < 400$ km, impulse or emergent onset. The wavelet front may be smoothed for increasing distance since absorption becomes dominant (Seidl and Stammler 1984). Pn is first arrival for larger epicentral distance, usually followed several seconds later by stronger Pg and PmP phase, if Pg is not yet

7

strongly attenuated at distances $\Delta < 400$ km. As a rule of thumb, Pn from a surface focus takes over Pg at $\Delta \approx 5\,z_M$, for deeper sources, however, at shorter distances.

* **PmP**: Has the largest amplitude of all crustal P phases because of total reflection from the Moho at overcritical incidence angles. PmP is never first arrival but follows very closely Pg (with $\delta t < 2$ s) after Pn has taken over as first arrival.
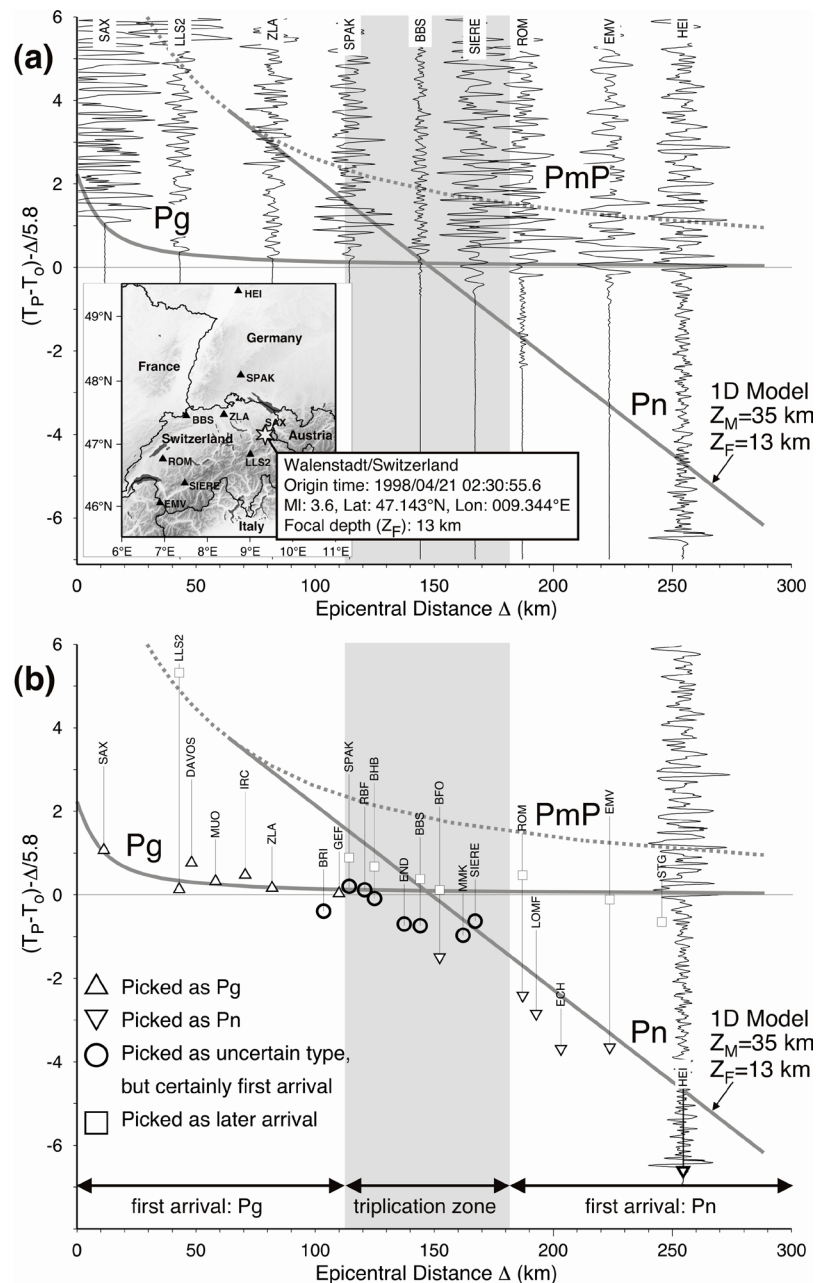
Figure 4a) Velocity-reduced record section of a local earthquake near Walenstadt, Switzerland. Amplitudes are normalised to maximum amplitude of each trace. Solid and dotted lines indicate synthetic travel-time curves for Pg, Pn, and PmP.
b) Velocity-reduced phase picks, crosschecked against synthetic travel-time curves derived from a simplified crustal model for the area under investigation (see text for discussion). Copy of Fig. 3 in Diehl et al. (2009, p. 545) with © granted by the Geophysical Journal International.

2.3 Phase Picking Part III: First-motion polarity and its error assessment

Information about first motion polarity is mainly needed for focal mechanism determination. Usually the polarity is denoted as 'Up' or 'Down'. Figure 1 represents an example for certain polarity identification. On the other hand, it is impossible to determine any polarity for the example of Figure 2. However, besides these two obvious cases, it is sometimes necessary to use an intermediate quality class for the first motion polarity. Time 'a' and 'b' in Figure 5 represent two possible positions for arrival time picks. In this case, the polarity is depending on the location of the pick. If the pick is assigned to position 'a', the polarity would be 'Up'. If position 'b' is used, the polarity has to be 'Down'. In both cases, we are not sure about the actual polarity, therefore we have to introduce an intermediate quality classes '+' or '-'. The error assessment scheme used here is summarized in Table 2.
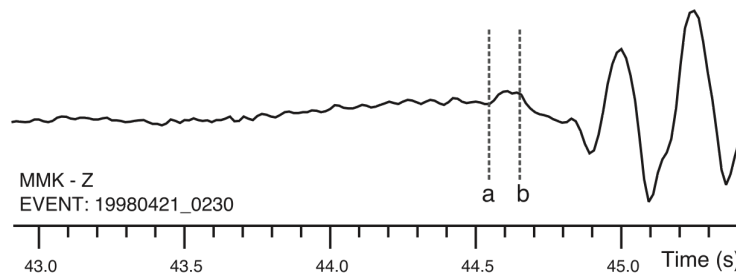

Figure 5   First-motion polarity and its error assessment: In this example the first-motion polarity is not independent from the pick position. If the pick is assigned to position 'a', the polarity would be 'Up'. If position 'b' is used, the polarity has to be 'Down'. In both cases, we are not sure about the actual polarity. Therefore we have to use the intermediate quality classes '+' or '-'.

Table 2 Error assessment used for first-motion polarity.

Polarity label	Polarity is…	Weight
U/D	Up/Down	Polarity is identified with certainty
+/-	Up/Down	Polarity is identified but uncertain
N	None	Polarity cannot be identified

2.4 Size of time window and amplitude scaling

The influence of time-window size and amplitude scaling on picking accuracy and phase identification as described e.g. by Douglas et al. (1997) is demonstrated in Figure 6a-d. In the uppermost example, the used time window is 5 s (Fig. 6a). The picked onset is labelled as P_a. For a narrower time window of 1.5 s, the onset at P_a seems a bit too late (Fig. 6b). Thus, we would pick the phase at position P_b in this window. The result is even more different, if the time window size remains the same, but the amplitude is multiplied by a factor of 5 (Fig. 6c) and 10 (Fig. 6d) respectively. An earlier phase is visible, which can be picked as P_c (Fig. 6d). But not only the absolute timing of the picked phase depends on window size and amplitude scaling, also the assigned uncertainty interval. The error interval might be smaller for the narrower time window and the magnified case.
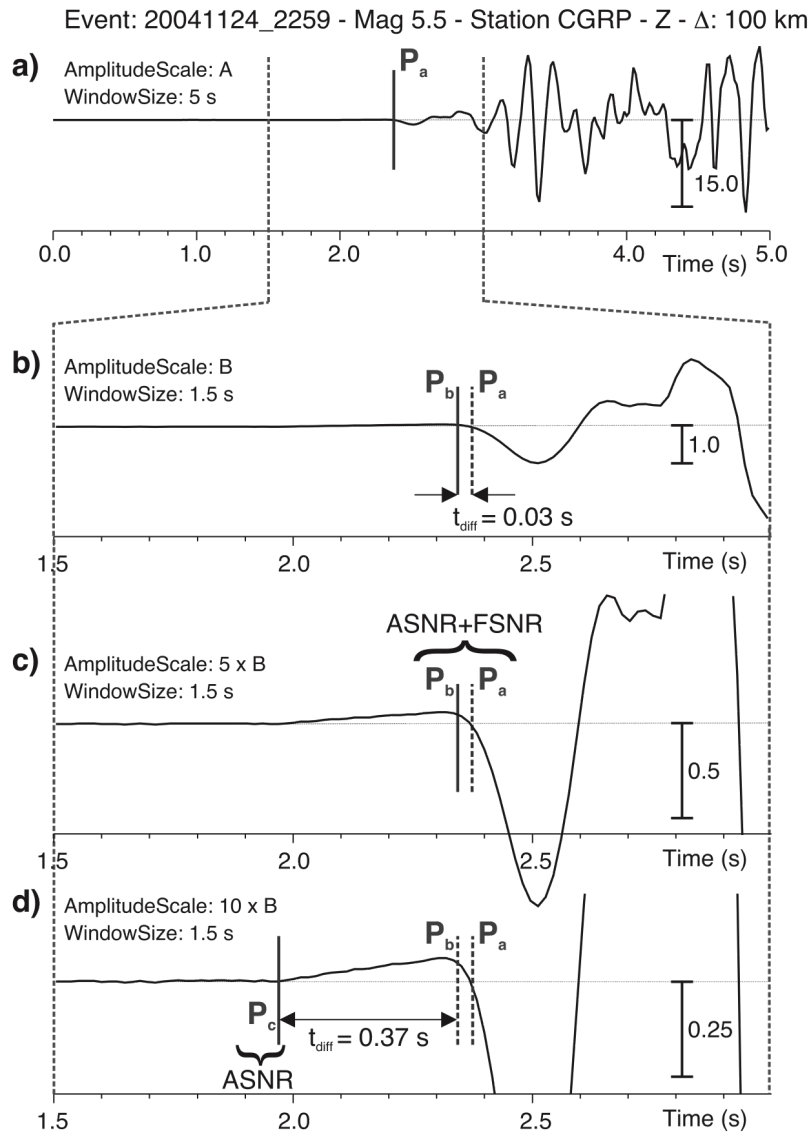
Event: 20041124_2259 - Mag 5.5 - Station CGRP - Z - Δ: 100 km

a) AmplitudeScale: A
WindowSize: 5 s

P_a

15.0

0.0   1.0   2.0   4.0   Time (s)   5.0

b) AmplitudeScale: B
WindowSize: 1.5 s

P_b P_a

1.0

$t_{diff} = 0.03$ s

1.5   2.0   2.5   Time (s)

ASNR+FSNR

c) AmplitudeScale: 5 x B
WindowSize: 1.5 s

P_b P_a

0.5

1.5   2.0   2.5   Time (s)

d) AmplitudeScale: 10 x B
WindowSize: 1.5 s

P_b P_a

P_c

$t_{diff} = 0.37$ s

0.25

ASNR

1.5   2.0   2.5   Time (s)

Figure 6 Different phase picking, caused by variable use of time window size (a, b) and scaling (c, d). See text for further discussion.

Considering the magnitude of the event, the small, ramp-like phase P_c in Figure 6 might be associated with the initiation of the fault rupture. P_c is obviously the first arriving phase, but it is arguable if it can be observed at stations with lower SNR (e.g., at larger epicentral distances). To obtain a consistent set of picks for the same earthquake it may be considered to pick the first prominent phase (P_b in Figure 6) instead. In contrast to the small precursory phase, the first prominent phase is expected to be observable at the majority of stations. Only precursors related to rupture complexities could be treated this way. Instead, P_c in Figure 6 might also be interpreted as the evolving Pn, taking over Pg as the first arriving phase. In this case, P_c has to be picked as the first arriving phase and cannot be ignored. Complexity of the source function usually scales with the rupture area. Therefore, small events (M<4) can be approximated as point sources in the far field and the shape of Pg is expected to be rather simple and impulsive. As mentioned earlier, an evolving Pn phase beyond the take-over distance between Pg and Pn can have the signature of a precursor signal. Similar effects are expected in subduction environments, where slab-phases are commonly observed. Such slab-

phases travel through the faster lithosphere of the subducting plate and manifest as precursors prior to the direct phase. Finally, it should be noted that interpretation of precursor signals requires the detailed knowledge of the complete instrument response as described in the following section. As demonstrated by Scherbaum (2001), precursor signals are often just artefacts of the instrument's anti-alias filter.

2.5 Aliasing and waveform filtering

From signal theory we know, that the correct digital representation of a continuous waveform depends on the sampling frequency. To avoid aliasing, a signal with frequency f has to be sampled with a sampling frequency $\Delta f > 2f$. Thus, the Nyquist frequency is defined as $f_N = 1/(2\Delta t) = \Delta f/2$. Any frequencies higher than f_N are aliased into lower ones. Therefore, we have to ensure that picking accuracy and phase identification will not be affected by sampling rates, which are rather small. As an example we consider a waveform sampled at $\Delta f = 20$ Hz or $\Delta t = 0.05$ s, which corresponds to a Nyquist frequency of $f_N = 10$ Hz. Concerning the observation error of a phase pick, the uncertainty intervals can not be smaller than the sampling interval. Therefore, the minimum picking uncertainty is defined as $\pm\Delta t$. To avoid possible inconsistency due to significantly different sampling rates used at different stations, we suggest to use only data with $\Delta f \geq 40$ Hz for local earthquake studies.

Aliasing occurs when the data are sampled, and once this occurs, the data cannot be 'unaliased'. Therefore, seismic data are usually filtered with an analogue anti-aliasing filter to remove frequencies above the Nyquist frequency before sampling. Furthermore, modern acquisition systems make use of oversampling and decimation techniques (Scherbaum, 2001; NMSOP Chapter 6). Such systems imply digital anti-alias filters, which often denote symmetrical or acausal impulse responses to avoid time shifting of the phases (zero-phase). As a consequence, the onset of very impulsive signals (also signal with frequency close to Nyquist frequency) may be obscured by 'acausal' precursory oscillations and their true onset becomes difficult, if not impossible, to determine. As an example for such precursors, Figure 7 shows the P-wave recording of a local earthquake near Davos, Switzerland (2006/10/24 13:08, Ml = 2.6) at the nearby station DAVOX.

In principle, this effect can be minimized by an inverse filtering process, described e.g. in Scherbaum (2001). However, this nontrivial procedure requires knowledge of the original anti-alias filter coefficients. Especially for large and inhomogeneous data sets, compiling the correct information can be rather difficult or even impossible. An alternative way to deal with this problem is to apply a consistent error assessment to it, as it is described above. The significance strongly depends on the amplitude scaling as discussed in 2.4 and low-pass filtering or integration of the signal may also help to reduce the amplitudes of such precursors. Since these precursors are present only for very impulsive and/or high-frequent wavelets, they are expected to be limited to recordings close to the epicenter and/or with low sampling rates and large relative bandwidth.
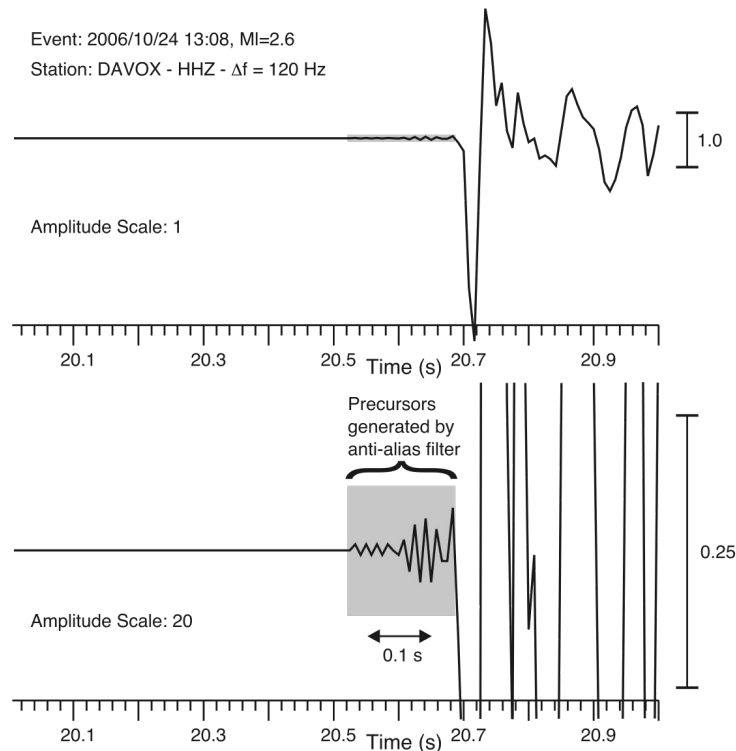
Figure 7 Precursors caused by acausal anti-alias filtering observed on the broadband registration of a local earthquake near Davos, Switzerland (2006/10/24 13:08, Ml = 2.6). Sampling frequency is 120 Hz. The precursors become obvious for enlarged amplitude scale (lower trace).

Filters are usually applied to enhance the SNR in the presence of noise. However, filtering can significantly change the true shape of the arriving wavelet and may also result in time-dependent phase shifts within the signal group (so-called "transient response"). These effects are particularly pronounced in narrow-band records (see section 4.2 in Chapter 4, e.g., Fig. 4.18). Therefore, care has to be taken when applying filters in the picking process. First of all, it should be noted that the original seismic record itself is the output of a filter (transfer function of sensor and digitizer), which distorts the true ground motion input depending on its relative bandwidth. Only a record of infinite bandwidth could reproduce the ground motion undistorted. Commonly used band-pass or high-pass filters not only reduce the amplitude of the noise, but can also result in distortion and phase shift of the signal. The phase shift introduced by a filter depends on the instrument response, the filter response and the frequency content of the signal. The closer the signal's dominant frequency is to the corner frequency f_c of the filter, the stronger the expected effect on the signal. Moreover, the steeper the flanks of the filter (higher order), the stronger are the expected effects on frequencies close to f_c.

Figure 8 demonstrates the effect resulting from the application of an arbitrary filter to a velocity proportional short period record. The corner frequency of the 2nd order high-pass filter (f = 1 Hz) is close to the dominant frequency of the first part of the wave group. Application of a 2nd order high-pass increases the effective steepness of the velocity proportional pass-band to the 5th order. This leads to an increased distortion of signals close to corner frequency, even for $f > f_c$ (see also Figures 7a and 7b in IS 5.2). As a result, the filter significantly affects the low-frequent part of the signal as demonstrated in Figure 8. Position

12

'a' and 'b' represent two possible arrival-time picks on the original and the high-pass filtered record. Time difference between the two positions could exceed 0.2 s, a value much larger than the uncertainty of each individual pick. Moreover, the filter process affects the first-motion polarity. A similar effect is demonstrated in Fig. 4.10 of Chapter 4.

In general, the use of filters has to be consistent for arrival-time picking. If broadband and short-period instruments are present in the same network, a common frequency band should be used to avoid inconsistencies between the two types of instrument responses. The application of a 2nd order high-pass with $f_c = 1Hz$ to a broadband record is appropriate to sufficiently simulate a short-period instrument response. Further practical guidelines for the use of filters are provided in section 3.1.
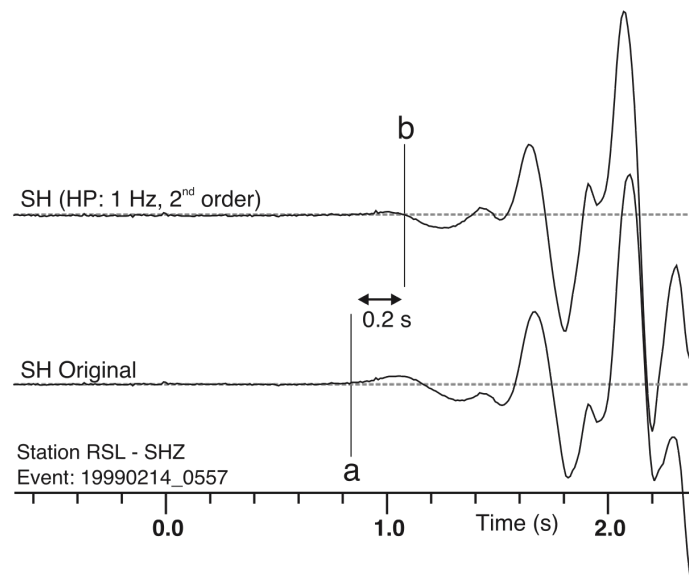

Figure 8 Effect of 2nd order Butterworth high-pass filter (1 Hz) on a short-period waveform. Note the significant change in waveform between the original and the filtered trace. The earliest low-frequency onset is hardly observable on the filtered trace. Position 'a' and 'b' represent two possible arrival picks for each trace with a time difference that exceeds 0.2 s. See text for further details.

2.6 Additional comments for S-wave picking

Most of the previous findings apply likewise to S-wave picking, however, identification and picking of S-waves is usually more difficult, since its onset is often superposed by the P-wave coda. Furthermore, we have to consider S-wave splitting due to possible seismic anisotropy and the presence of Sp-converted precursors due to the presence of shallow strong velocity discontinuities.

2.6.1 Polarization of the wavefield

According to linear theory of wave propagation in homogeneous isotropic media P and S waves are fully independent solutions of the equation of motion results with linear particle motion. Figure 9 illustrates the particle motions of P and S waves in the horizontal (a) and vertical (b) planes of wave propagation. The particle motion of the P wave is parallel (or

longitudinal) to the direction of wave propagation vector $\mathbf{k}$. In contrast, the displacement field of the S wave is transverse to $\mathbf{k}$ and can be subdivided into a vertical component (SV) and a horizontal component (SH). The vector $\mathbf{k}$ can be described in the Cartesian ZNE-system of the seismometer (vertical, north-south, east-west) by two angles: the backazimuth (*BAZ*) and the angle of incidence (*i*). Both angles can be determined from polarization analysis of a three-component recording in a window around the P-wavelet. If station and epicenter coordinates are known, *BAZ* can also be derived from the orientation of the great-circle including station and epicenter. If focal depth and epicentral distance are known, we can also determine the theoretical angle of incidence in a given velocity model. However, in real inhomogeneous Earth the true arrival angles *BAZ* in the horizontal and *i* in the vertical plane depend on frequency and thus wave length (see Fig. 2.6 in Chapter 2 and Fig. 11.23 in Chapter 11).
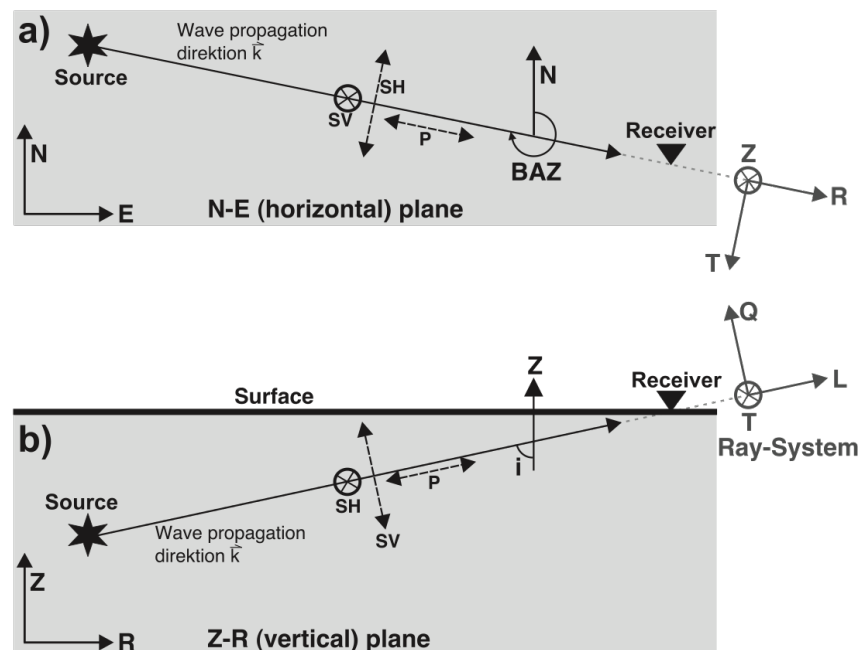

Figure 9 Particle motion for P and S wave along wave propagation direction a) in the horizontal plane and b) in the vertical plane.

Both angles can be used to rotate the ZNE coordinate system into a local ray-system. Within the ray system P, SH, SV components can be partly separated from each other. The horizontal rotation of ZNE by *BAZ* results in the ZRT-system as demonstrated in Figure 9a.

The T-component denotes the transverse component, i.e., perpendicular to the direction of wave propagation in the horizontal plane, R coincidences with the radial component, i.e., in the horizontal direction of wave propagation. In the ideal case of a flat-layered isotropic medium, the T-component contains only SH energy. P- and SV-energy are still mixed on Z and R to a variable degree, depending on the incidence angle *i* and the source mechanism (see Chapter 3). An additional rotation of ZRT by the incidence angle *i* results in a decoupled ray-system LQT. The complete P-wave energy is then recorded on the L-component (longitudinal) and the Q-component contains the SV energy only. The T-component remains the same as in ZRT.

Since both P and SV are polarized in the vertical plane of propagation, SV-wave energy incident on a velocity discontinuity can partly be converted into a P wave during reflection at or transmission through such an interface (or vice versa P into SV). If such an interface is close to the surface and denotes a strong velocity contrast (e.g. basement-sediment interface), Sp precursors are generated, which then arrive shortly prior to the initial SV-wave. These Sp precursors may be misinterpreted as a too early onset of the S-wave. The use of a ray-system can be used to identify such precursors, as demonstrated in Figure 10. Sp precursors are not present on the T-component, since there is no coupling between SH and P. However, the ratio between radiated SH and SV energy strongly depends on the focal mechanism and its orientation in space and thus also on the observation azimuth.

To avoid the misinterpretation of Sp precursors as the true S-wave arrival we recommend the use of a ray system (ZRT or LQT) and pick the S wave preferable on the T-component. Furthermore, the use of a ray-system can be helpful for a better discrimination of S energy generated by the P coda and to identify phases like Sn as demonstrated in Figure 10. In addition, the application of a Wood-Anderson simulation filter (high-pass with $f_c = 1$ Hz in combination with an integration from velocity to displacement) can be useful to enhance the S-wave onset. The final S-pick, however, should be crosschecked with its position on the velocity proportional record.
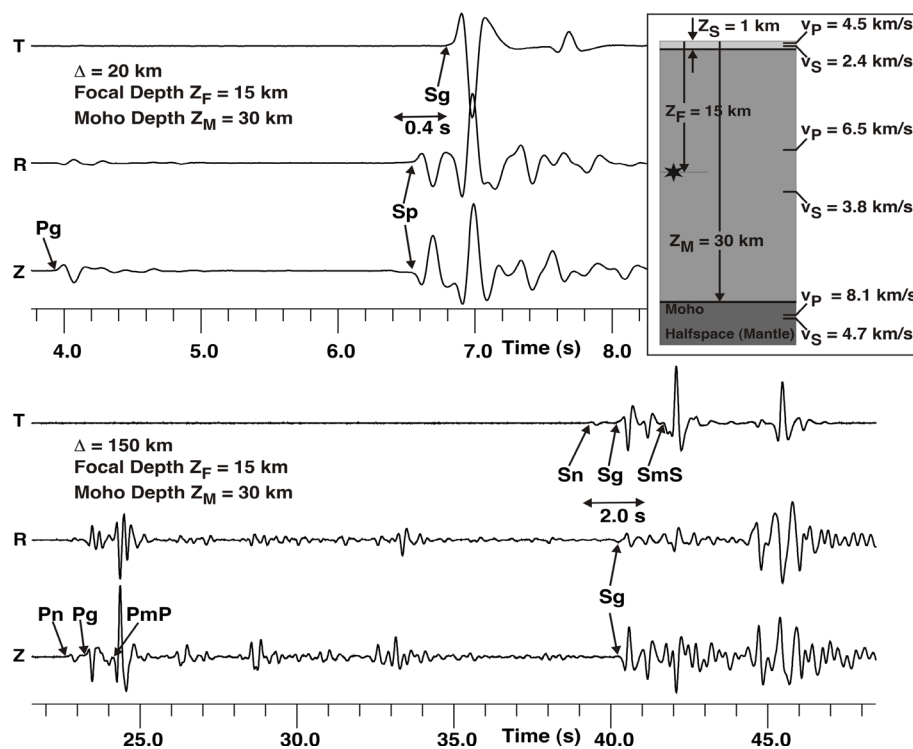

Figure 10 Theoretical seismograms calculate by the reflectivity method of Fuchs and Müller (1971) for a simplified 1D crustal model (upper right inset) using the *refmet* code provided by T. Forbriger. The uppermost layer represents a sedimentary basin of reduced P- and S-wave velocities. The uppermost traces show vertical, radial and transverse component at a distance of 20 km. The Sp precursor phase is clearly visible on Z and R component. The lowermost traces correspond to a distance of 150 km. The amplitude of the first arriving Sn phase is rather weak compared to later arrivals (Sg, SmS) and only visible on the T component. All amplitudes are normalized by the calculated maximum record amplitude for the considered station.

15

Another form of S-wave "splitting" results from travelling through anisotropic Earth material. In such media part of the SV-wave energy is coupled with some time shift into the T component, producing instead of a linear SV motion a more or less elliptical S-wave motion in the R-T plane. The degree of ellipticity and the amount of time shift between the related S onsets in the R and T component depend on the degree of anisotropy of the medium through which the S wave is travelling. Furthermore, the time shift depends on the angle between the anisotropy axis and the incident angle of the S wave and therefore it depends also on the epicentral distance. This allows to determine the degree of (specifically horizontal) anisotropy and its orientation in space by restoring iteratively the linear motion of SV expected for isotropic media. This is illustrated, e.g., by Fig. 2.7 in Chapter 2 for teleseismic SKS waves. The time shift between the first S arrivals in R and T may range between several tenths of seconds and several seconds, depending on what type of S waves one analyzes at which frequencies and source distances and with focus on which parts of the Earth (e.g., crust, upper mantle or deeper). Also in this case it is helpful to analyse arrivals in the S-wave range and their polarization in a ZRT or LQT system in order to discriminate between onsets in different components due to wave conversion at a discontinuity or caused by true S-wave splitting due to travel through anisotropic Earth material.

3. Consistent hand picking procedure

The findings discussed in the previous sections will be combined to a standard procedure for consistent P- (and S-) phase picking in the following sections. This requires, first and foremost, that the picking is made on some standardized type of seismic record and that time window length and the amplitude scaling are chosen consistently. Therefore, we will discuss in detail these major sources for inconsistent picking.

3.1 Consistent waveform filtering

As demonstrated in section 2.5, filtering may lead to inconsistent picking. Therefore, we suggest the following guidelines:

- The original seismic record itself is the output of a filter, which distorts the true ground motion input depending on its relative bandwidth. Only a record of infinite bandwidth could reproduce the ground motion undistorted (see Chapter 4).

- Since for local/regional applications emphasis is on high-frequency signals one should preferably use either directly original short-period (SP) records or filter BB records accordingly so that the lower corner frequency f_{cl} of the passband is about 1 Hz.

- Short-period (SP) channels (EH, SH):
  Typical SP sensors are electromagnetic seismographs of the geophone type with a seismometer eigenfrequency $f_S \approx 1Hz$ (or higher). They have a response proportional to ground motion velocity between $f_S = f_{cl}$ (lower corner frequency) up to the corner frequency f_{cu} of the anti-aliasing filter. If $f_{cu} = 10$ Hz, respectively 50 Hz (i.e., if the data are sampled with $\Delta f \approx 40$ Hz, respectively 200 Hz) then this corresponds to a velocity-proportional relative bandwidth (RBW) between some 3.5 to 5.5 octaves or 1 to 1.7 decades. Note that this is much less than for modern broadband seismographs,

which also have a velocity-proportional response but within the range $f_{cl} \ll 1$ Hz (up to ≈ 0.3 mHz) and $f_{cl} \approx 10$ to 20 Hz (with $\Delta f \geq 40$ Hz), corresponding to an RBW between some 2 to 4 decades. Note, however, that the RBW of common bandpass-filtered SP seismographs used for teleseismic observations is only about 1 and 2 octaves (e.g., Fig. 4 in Granville et al., 2005) and should not be mistaken with the SP sensors considered here for local and regional travel-time studies.

- To avoid aliasing-effects, be sure that the upper corner frequency f_{cu} of the filter is well below Nyquist frequency, typically at $\leq 1/4^{th}$ of the sampling rate Δf and with a steep roll-off for $f > f_{cu}$.

- Unfiltered SP sensors have already a limited bandwidth with a step 3rd order roll-off of the response for $f < f_{cu}$ (see Fig. 5.3 in Chapter 5) which results in significant phase shift and distortion of the earliest parts of the waveform (for frequencies up to about 3-4 times f_{cl}).

- Therefore, one should avoid further frequency filtering when ever possible. Apply a 2nd order 1 Hz high-pass filter only if necessary, e.g. in presence of low-frequency noise. This filter will not affect the velocity-proportional passband, yet be aware that it will steepen the roll-off for $f < f_{cl}$ to 5th order, thus causing larger phase shifts and waveform distortions up to $f \gg f_{cl}$. Therefore, compare original waveform with filtered one before final picking. Also check, if the filter changes first motion polarity.

- Apply possible low-pass or band-pass filters only if necessary, e.g., in presence of high-frequency noise. Compare original SP waveform with filtered one before final picking.

- Broadband (BB) channels (HH, BH):
  Modern feedback-controlled BB seismographs are widely in use now. They have also velocity-proportional response for $f > f_{cl}$ (see Fig. 11.27 in Chapter 11). If one applies a high-pass filter with corner frequency 1 Hz to such a wider broadband records with $f_{cu} \ll 1$ Hz it will remove the long-period noise often present in BB recordings, and in addition, will simulate well the response of an original 1 Hz SP record of the geophone type. Thus, filtering BB records with a constant $f_{cu} = 1$ Hz will minimizes the inconsistency due to different types of BB sensors used in practice.

- S-wave identification and picking:
  Application of a Wood-Anderson simulation filter ($f_{cl} = 1$ Hz in combination with an integration from velocity to displacement) can be useful to enhance the S-wave onset. In addition, component rotation to the RT-system can help to identify the S-wave on the T-component.

3.2 Consistent window size and amplitude scaling

A uniform procedure is required to minimize subjectivity in phase picking due to irregular choice of time window size and amplitude scaling as shown in Figure 6. On the other hand, it turns out to be very difficult to define universal rules, especially, if the method should be feasible for picking of large data sets. A consistent choice of time window and amplitude

scaling should satisfy two conditions: A fixed time window length and amplitude normalisation with respect to a reference scale.

As already mentioned, universal rules for these conditions are difficult to define. Concerning the time window length, the choice depends on the dominant frequency of the signal, but also on the *ASNR*. In the presence of strong noise or in the case of a weak and emergent signal, it is often better to use a broader time window to determine the change in frequency and follow the transition from the signal to the noise part. In addition, many picking tools normalise the amplitude to the maximum amplitude within the selected time window and therefore amplitude scaling depends also on the size and the position of the time window. A possible approach to minimize the inconsistency related to time window choice and amplitude scaling may consist of a mixture of iterative selection of window sizes and sliding them stepwise from the signal part towards the noise dominated part. For a further description, we apply this approach to the example shown in Figure 6. A priori, we define four possible time windows used for picking:

Length of **H**igh-**R**esolution **W**indow (HRW):	2 s	$ASNR \geq 3$
Length of **M**id-**R**esolution **W**indow (MRW):	5 s	$2 \leq ASNR < 3$
Length of Low-**R**esolution **W**indow (LRW):	10 s	$ASNR < 2$
Length of **V**ery-low-**R**esolution **W**indow (VRW):	15 s	

In the first step we choose a broad overview window, which includes the whole coda of P or even parts of the S-coda (Fig. 11a). 'P-PRED' denotes the theoretical arrival time predicted in a velocity model for a preliminary hypocenter. The predicted arrival time can be useful, but only as a rough guide and is not necessary. We pick the approximate position P_{aprox} of the earliest arrival visible in this window. Based on P_{aprox}, the maximum noise and signal+noise amplitude is estimated. To avoid parts of the signal in the noise window, we define a safety gap of ±0.5 s around P_{aprox}. We use a length of 3 s for the noise window and of 0.5 s for the signal+noise window. We define the noise threshold as ±1.5 times the absolute noise amplitude within the noise window. In addition, we calculate *ASNR* from the absolute noise and signal+noise amplitudes. Depending on the resulting *ASNR*, we choose the appropriate window size as described above.

In Figure 11b *ASNR* is several times larger than 3, therefore we use the HRW-size for picking. Between Figure 11b and 11e, the time window is shifted stepwise towards earlier times. The maximum amplitude within each time window is used for amplitude scaling. As long as the upper and lower noise threshold (dashed horizontal lines) are close to each other, the time window can be shifted further to earlier times (i.e. enlarging the amplitude scale). Finally, in Figure 11e, the amplitude scaling allows an almost perfect discrimination between noise and signal. In this example, the suggested procedure prevents missing the small precursors. If we could not clearly distinguish between noise and signal with the actual window size, or if we are not sure whether it is definitely the first arrival (e.g., in the presence of strong noise), we repeat the sliding procedure with a larger time window (MRW or LRW). Subsequently, we apply the consistent error assessment as described in section 2.1 to determine t_L, t_E, and t_A. The upper and lower noise thresholds (dashed horizontal lines) are used for the consistent determination of t_L.
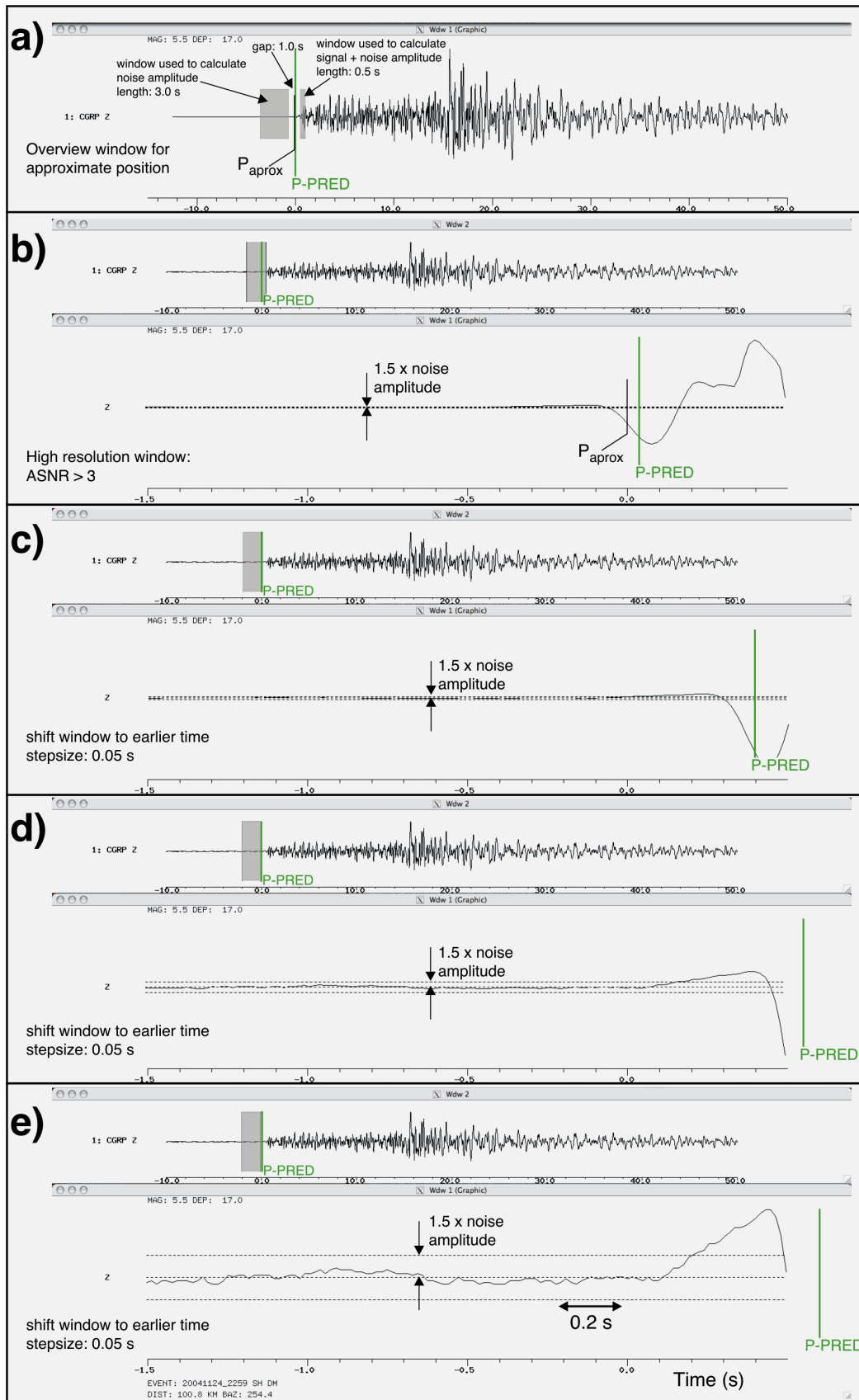
Figure 11 Sliding time window procedure used for consistent phase picking. See text for further details.

3.3 Consistent phase identification

Provided that a hypocenter can be calculated, the actual phase identification can be crosschecked against a simplified crustal model (similar to Figure 4b). Another helpful tool to minimize inconsistency due to phase misinterpretation can be the use of synthetic or predicted arrival times, especially for re-picking of seismograms. However, as the comparison of Figures 3 and 4 shows, the actual phases may look very different and also their onset times may significantly deviated from the synthetic ones. Therefore, one should never pick the onsets at the theoretically predicted arrival times and identify the phase on waveform synthetics, unless all the subsequently applied criteria for phase identification and picking, as described above, are sufficiently well fulfilled. Because our goal is not to confirm already existing, usually grossly simplified 1-D models but to substitute them by high-resolution 2- and/or 3-D models by picking well-established deviations of correctly identified real phase onsets from theoretically predicted ones.

If, however, a reasonably accurate local or regional velocity model is available and a preliminary hypocenter has been calculated on the basis of such a model, we can calculate synthetic first arrival times for each event-station pair, prior to the picking process. This provides three major advantages. First, they may guide the picker to the right phase (but as said above, with the reliability depending on model quality) and thus reduce phase misinterpretations. Second, the synthetics can also be used to arrange the seismograms according to their expected arrival times. Thus, one can start the picking at the closest station and does not waste too much time with likely low quality arrivals. In addition, the synthetics may give at least some rough guidance for recognizing and tracking possible, theoretically expected changes in waveforms from station to (neighbouring) station. Third, it represents a rough test for correct synchronization of the timing system. In case of obvious timing errors of a station, we would observe a large discrepancy between synthetic and actual waveform arrival.

Acknowledgments

References

Bormann, P., Klinge, K., and Wendt, S. (2002). Data analysis and seismogram interpretation. In: Bormann (ed), *IASPEI New Manual of Seismological Observatory Practice (NMSOP)*, GeoForschungsZentrum, Potsdam, ISBN 3-9808780-0-7, Vol. 1, Chap. 11, 100 pp. or http://nmsop.gfz-potsdam.de.

Di Stefano, R., Aldersons, F., Kissling, E., Baccheschi, P., Chiarabba, C., Giardini, D. (2006). Automatic seismic phase picking and consistent observation error assessment: Application to the Italian seismicity. *Geophys. J. Int.*, 165, 121–134.

Diehl, T., Kissling, E., Husen, S., Aldersons, F. (2009). Consistent phase picking for regional tomography models: application to the greater Alpine region, Geophys. J. Int. 176, 542–554.

Douglas, A., Bowers, D., and Young, J. B. (1997). On the onset of P seismograms. *Geophys. J. Int.*, **129**, 681–690.

Fuchs, K., Müller, G. (1971). Computation of synthetic seismograms with the reflectivity method and comparison with observations, Geophys. J. Roy. Astron. Soc., 23, 417–433.

Husen, S., Diehl, T., Kissling, E. (2009). The effects of data quality in local earthquake tomography: Application to the Alpine region. *Geophysics*, **74**, WCB71-WCB79.

Kulhánek, O. (1990). Anatomy of seismograms. *Developments in Solid Earth Geophysics* **18,** Elsevier, 78 pp.

Kulhánek, O. (2002). The structure and interpretation of seismograms. In: Lee, W. H. K., Kanamori, H., Jennings, P. C., and Kisslinger, C. (eds.), *International Handbook of Earthquake and Engineering Seismology*. Academic Press, Part A, 333–348.

Scherbaum, F. (2001). Of poles and zeros: Fundamentals of Digital Seismology. *Modern Approaches in Geophysics*, Kluwer Academic Publisher, 2nd edition,.

Scherbaum, F. (2002). Analysis of digital earthquake signals. In: Lee, W. H. K., Kanamori, H., Jennings, P. C., and Kisslinger, C. (eds.), *International Handbook of Earthquake and Engineering Seismology*. Academic Press, Part A, 349–355.

Seidl, D., Stammler, W. (1984).Restoration of broad-band seismograms (Part I). *J. Geophys*., **54,** 114–122.

Simon, R. B. (1981). Earthquake interpretations: A manual of reading seismograms. William Kaufmann Inc., 150 pp.,

Stammler, K. (1993). Seismic Handler – programmable multichannel data handler for interactive and austomatic processing of seismological analysis. *Comp. Goesci*., **19**, 135-140.

Wessel, P., and Smith, W. H. F. (1995). New version of the Generic Mapping Tool released. *EOS, Trans. Am. Geophys. Un*., **76**, 329.